This article has been accepted for publication in a future issue of this journal, but has not been fully edited. Content may change prior to final publication. Citation information: DOI 10.1109/TIA.2015.2499287, IEEE Transactions on Industry Applications

Optimized Resource Management for PV-Fuel Cell Based Microgrids using Load Characterizations

F. Cingoz, *Student Member, IEEE*, A. Elrayyah, *Member, IEEE*, and Y. Sozer, *Senior Member, IEEE*
School of Electrical and Computer Engineering
University of Akron
Akron, OH

***Abstract*—Maintaining a reliable and cost effective operation in microgrids has significant importance. One factor required for optimal operation of the microgrid is to keep a certain energy reserve without unnecessary cost to satisfy load variations. In this paper, an optimal reserve assessment of photovoltaic and fuel cell based microgrids are investigated while considering reliability and economic aspects. A typical residential load is predicted to introduce an optimal power sharing approach, and accordingly, to achieve reliable and cost effective system operation. Load sharing between sources in microgrids affects the cost, and also affects the source's ability in responding to load variations. A nonlinear frequency droop scheme is then used as a tool to achieve the optimization objectives such that the operating cost is minimized without jeopardizing the microgrid's ability of responding to sudden load variations. Presented results confirm the validity of the power sharing approach and verify its effectiveness and feasibility.**

I. INTRODUCTION

Industrial and economic development over the world has increased fossil fuel consumption in the last century. Conventional fossil fuel based energy sources have presented a satisfying solution to the energy demand in the past; however, environmental pollution and global warming due to the increase in global greenhouse gas emissions have become genuine threats for all living creatures. According to a recent U.S. Energy Information Administration (EIA) report, the world net energy consumption is predicted to increase by more than 85% from 2010 to 2040 [1]. The impact of greenhouse gas emissions could then become more serious in the future unless environmentally friendly sources become widely adopted. Therefore, there is a need to increase the penetration of renewable energy in energy systems to decrease the dependency on fossil fuels and consequently reduce greenhouse gas emissions.

Renewable energy sources (RESs) do not only provide pollution-free energy, but also offer efficient and high-quality energy production. Moreover, the cost of RESs has decreased significantly in the last three decades. Accordingly, the growth rate of RESs' generation capacity has increased rapidly over the years as shown in Fig. 1(a). As one of the most widely deployed renewable energy technologies, solar photovoltaic (PV) is considered to be a promising energy source. Figure 1(b) shows the current and the predicted U.S. electricity generation capacity of PV sources and their status among the other RESs.

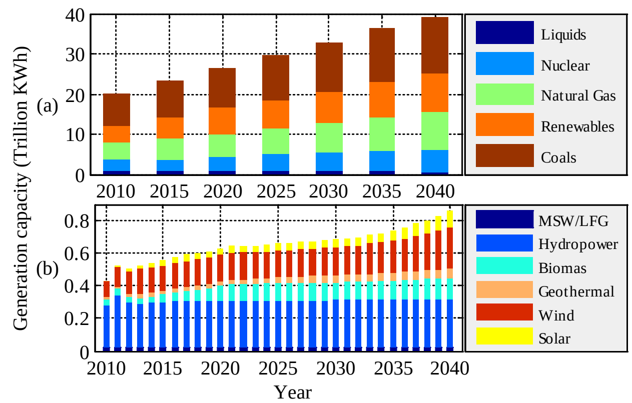

Figure 1. (a) The recent history and future projected profiles of world electricity generation (b) and of U.S. renewable electricity generation by different type of sources [1].

The global PV market is continuously growing as PV sources present distinguishing benefits such as easy installation, little maintenance, and high-quality performance. In particular, they can be installed almost anywhere at any desired capacity. These advantages make PV sources one of the best candidates for powering residential and commercial sectors. Since nearly 40% of the total world annual energy consumption is taken by residential and commercial sectors, PV sources can play an important role in satisfying the world energy-demand growth [2]. However, PV systems cannot be used as the sole source in a power system since they cannot produce electrical energy at night. Thus, alternative energy sources such as fuel cells (FC), micro turbines (MT), and diesel generators are suggested to be combined with PV sources to achieve more reliable, efficient, and sustainable energy [3-5]. Since the PV sources run with zero fuel cost, they are generally preferred to be operated at their maximum power points (MPPs) to achieve maximum efficiency [6-8]. Any excessive electrical power generated by the PV source is stored in energy storage elements to increase the overall system efficiency. The storage elements increase power quality by compensating sudden load variations in the case of insufficient power generation by the PV sources.

Conventionally, PV sources are connected to microgrids as secondary suppliers in small-scale. In this paper however, PV sources are considered to be the primary sources with relatively higher capacity than other sources integrated into the microgrid, as power suppliers for residential loads in particular. Residential microgrids are solutions to integrate more RESs behind-the-meter such that utilities operators can be relieved from the burden of managing the RESs in power systems. Accordingly, in the residential microgrid, there is a need to secure a supply of power which matches load variations. Emerging technologies like plug-in-hybrid-vehicles (PHV) are expected to play an active role in responding to sudden load variations since its batteries can be used when needed. However, during the day time, as PHVs are expected to be unavailable in residential microgrids, there is a need for another type of reserve. Clearly, storage elements could be installed specifically for that purpose in a residential microgrid, however the cost issue remains as an impeding factor.

It would be an interesting study to investigate whether there could be some scenarios where it is more cost effective to oversize the PV installation in a certain microgrid rather than installing battery storage elements [9]. In this case, the PV sources could be operated when needed in non-MPP operation mode, allowing the PV production to increase, thus satisfying any sudden load variation. This investigation requires a comparison methodology between the PV and battery cost and to propose a certain control algorithm that drives the PV sources, taking the natural load variation into consideration. These two points are covered in detail in this paper.

As the first point of this paper, it is suggested that PV sources should produce less power than the power given at the MPP. This reserved energy in the PV source could be effectively utilized to compensate the rapid residential load variations and/or power fluctuations of the PV source. However, the cost then becomes a decisive factor in determining the capacity size and, accordingly, the reserve maintained in the PV operating point.

PV sources cannot supply additional power when the demand increases if they operate at MPP. Then, power mismatch between production and consumption may take place during load variations or power fluctuations of the PV source due to atmospheric changes. In conventional microgrids, alternative sources operated in parallel with PV sources can respond to power mismatch at a reasonable rate. However, in microgrids, where PV sources are highly penetrated, power systems may experience more drastic power mismatches. Since alternative sources such as FC and MT have relatively slow response, they may not be able to compensate such drastic power mismatches before the power system collapses. Energy storage devices such as batteries and supercapacitors have been proposed as solutions to the power mismatch issue because they offer relatively fast response times [10-12]. However, as the PV source rating increases, the control and management of the PV source requires an equivalent increase in the energy storage system. That may increase installation cost of the microgrid system significantly due to the high capital cost of storage devices.

In this paper, a microgrid system consisting of a PV source integrated into an FC will be studied. FC is typically considered as a back-up source during the daytime, but it behaves as a primary source during the night as some applications require. In this study, an analysis is considered for fuel cells with PV as it represents a suitable selection for systems which require large energy capacity, but not necessarily large power capacity supported by the ESS. In the literature, research has been presented on the reliable operation and management of the PV-FC hybrid system [5], [13]-[16]. The general control concept for PV sources in these studies is to utilize the MPP technique effectively while ensuring the reliable operation of the FC. In [13], [15], [16], batteries are used as energy storage devices to compensate the slow response of the FCs and to store the excessive energy generated by the PV sources. The studies show that the size of the storage devices increase with the size of the PVs, which increases the total cost of the system considerably due to the high cost of storage devices [19]. The increasing need of storage devices raises the question of designing the optimal storage size for certain applications [15]-[19]. As opposed to the existing studies, this paper studies the case of a PV-FC system without ESS by operating the PV system at non-MPP operation. Moreover, the dynamic power sharing among the sources is performed using nonlinear droop relations designed through load modeling. Including the load modeling and characteristics in designing the nonlinear droop relation provides a mean to optimize the resource allocation and system operation. The paper shows a different way to operate RES sources while considering new factors to manage their operation.

The non-MPP operation enables PV sources to have some headroom power (Δ_p), which later can be utilized as an energy reserve for the system in the case of any power mismatch. Since the response time of PV sources is relatively faster than some other alternative sources, the microgrid system can offer more reliable and sustainable power generation by utilizing headroom power offered by PVs. Also, the negative effect of power fluctuation during atmospheric changes can be significantly reduced by keeping a Δ_p for PVs. On the other hand, the productivity of the PV source decreases as the headroom power increases, which affects the operation cost of the system. Moreover, the lack of an ESS raises the question of how to manage the excessive PV power properly. In order to address these issues, optimal headroom power reserve is first studied by characterizing the load data. Then, a control method is provided to perform a PV-FC operation with optimal headroom Δ_p and with zero storage capacity while maintaining desired system reliability with minimum cost. After proving the concept, the optimization between the headroom size Δ_p and the storage element size can then be analyzed.

The organization of the paper is as follows. In section II, first, reliability and cost analysis of a microgrid system is discussed to address the effect of the headroom power. A methodology is

This article has been accepted for publication in a future issue of this journal, but has not been fully edited. Content may change prior to final publication. Citation information: DOI 10.1109/TIA.2015.2499287, IEEE Transactions on Industry Applications

proposed to optimize the value of the headroom power so that a microgrid can operate at a desired reliability level while minimizing the running cost. This section is closed with an investigation of the cost effect of an ESS for the considered microgrid scenario. In Section III, a nonlinear droop frequency is proposed to achieve desired power sharing between the sources in the microgrid and to stabilize the system frequency. The effectiveness and feasibility of the proposed method is verified by simulation and experimental studies in Section V.

II. Reliability and Cost Analysis

The power production of PV sources is highly dependent on atmospheric conditions such as irradiance and temperature. Therefore, unpredictable changes in climate (e.g., passing clouds and morning fog) may cause sudden fluctuations in the output power, which may also result in voltage and frequency disturbance in the power network [22]. Due to the intermittent power production, the control and power management of PV systems becomes more challenging as PV systems' penetration increases. One provided solution to this problem is to operate the PV sources in a microgrid. Microgrids are controllable electrical networks that comprise of distributed power sources, energy storage devices and loads [23]. Basically, distributing the PV sources over the microgrid simplifies the control and management of the power flow. This increases the performance of the PV sources and the reliability of the power network [13, 24]. In microgrids, if PV sources are utilized as the primary source during the daytime, the microgrid system may suffer from sudden load variations and unpredictable power variations of the PV sources. Therefore, it is suggested that PV sources should operate at operating points other than their MPP to leave some Δ_p as an energy reserve. This reserved energy may increase the system reliability due to the following reasons:

- PV sources operating at their MPP cannot assist in supplying additional power to the microgrid in the case of load variations. PV sources operating with Δ_p can use the reserved power to satisfy the load variations in the microgrid during the daytime.
- The output power fluctuations of PV sources may disturb the microgrid if the PV sources are operated at their MPPs. As demonstrated in Fig. 2, the insulation variation from λ_1 to λ_2 leads to power fluctuation from the operating point x1 to x2. If PV systems consisting of many PV modules are considered, this power variation can be considerable. On the other hand, the PV sources operating with Δ_p could experience less power fluctuation from operating point y1 to y2 corresponding to the same insulation change as shown in Fig. 2. The decrease in power fluctuations can reduce the negative effect of atmospheric changes on PV sources and accordingly on the microgrid system.

On the other hand, keeping Δ_p decreases the productivity of the PV source and accordingly increases the PV system's operating cost. The trade-off between reliability and operation cost raises a question of determining the optimal value of Δ_p such that the microgrid system can satisfy the desired reliability level at various loading conditions while maintaining the optimal operating cost. In order to investigate the operation of PV sources with a Δ_p reserve, a case study of a microgrid is considered in the following subsection.

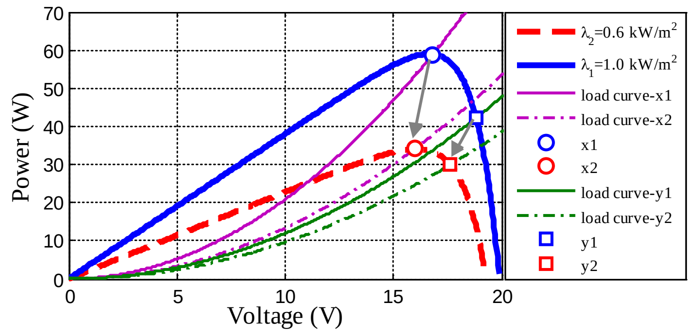

Figure 2. Voltage-power characteristic of a PV module at different insulations.

A. Microgrid system configuration

Several research studies have been presented on the operation and management of the PV-FC hybrid system [5], [13]-[16]. In this paper, a PV source is designed as the primary source during the daytime, while an FC is assumed as a secondary source. Here, the FC plays an important role in compensating the required load demand when the PV production becomes insufficient. As a case study, the residential PV-FC based microgrid power generation system is considered as shown in Fig. 3. The details regarding modeling of the PV and FC sources and the implementation of control strategies can be found in [25-30]. The sources are first sized based on the selected load profile. The load power (P_{load}) for the intended residential area is around 3 kW, but it may occasionally have peaks up to 9 kW during the daytime. The rated power of the PV sources is set to 3.6 kW at an insulation level of 1 kW/m^2 while the FC is rated for 6 kW.

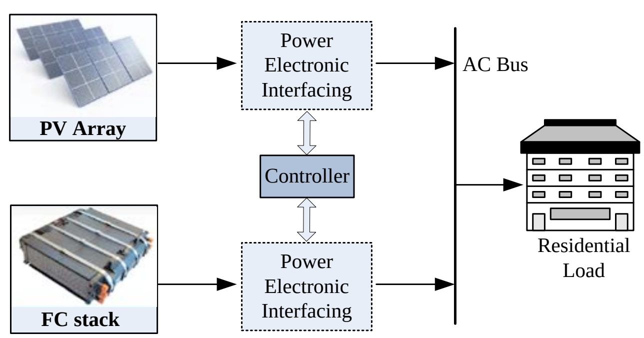

Figure 3. Overall configuration of the PV/FC power generating system.

The objective is to operate the microgrid system at the desired reliability level while optimizing the overall operating cost. This

This article has been accepted for publication in a future issue of this journal, but has not been fully edited. Content may change prior to final publication. Citation information: DOI 10.1109/TIA.2015.2499287, IEEE Transactions on Industry Applications

objective can be achieved by performing the following tasks in two stages:

- In the first stage, Δ_p values for all potential loading conditions must be determined to satisfy the determined reliability levels.
- In the second stage, Δ_p values need to be found for all potential loading conditions to minimize the operating cost of the considered microgrid.

Based on the results achieved from these two stages, optimal Δ_p values which minimize the cost without violating the selected reliability level can be determined for all loading conditions.

B. Reliability aspect

Typically, drastic load variations in residential sectors only occurs when the power system operates at specific loading conditions. It can be concluded that the magnitude of the load variations depend on the system operating point. To find the optimal value of Δ_p, predictions for the load variations have to be obtained. These predictions are obtained by modeling the load variation as a random variable with a certain probability density function (pdf). To increase the effectiveness of the presented method, the load is divided into intervals and the pdf of every interval is obtained.

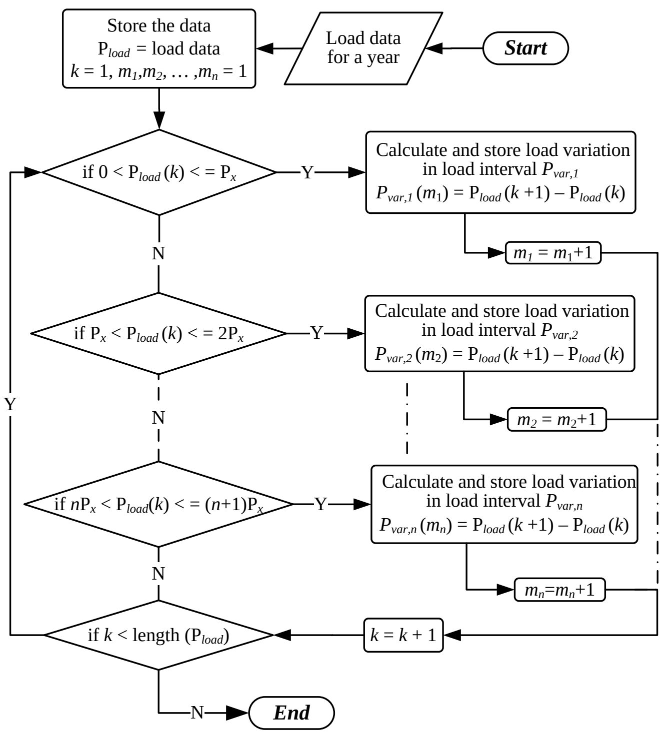

Figure 4. Flowchart of load variation data acquisition for different power intervals.

The flow chart in Fig. 4 demonstrates the procedure of finding the pdf of a load variation. First, the number of considered intervals n is selected. This number is a tunable parameter based on the load variation characteristics. The amount of power in every interval then becomes $P_x = P_{load}/n$. To determine the pdfs of the load variation, the load data is observed. For every loading condition, the corresponding load interval is determined as shown in Fig. 4. When the load changes within that interval, the value of the variation is stored for later processing. After accumulating a sufficient number of samples, the pdf of each interval can be developed.

The load variation values stored in each data set has been modeled as a random variable with normal distribution. The mean and standard deviation values of these distributions have been statistically obtained from the saved samples. These values can be used in a pdf to observe the Gaussian probability distribution of each data set representing different load intervals. The Gaussian probability distribution is one of the most commonly used continuous probability distributions. The pdf of a random variable with a Gaussian distribution is given by:

$$f(x) = \frac{1}{\sigma\sqrt{2\pi}} e^{-\frac{(x-\mu)^2}{2\sigma^2}} \qquad (1)$$

where x is a continuous random variable ranging in $[-\infty, +\infty]$. The Gaussian distribution is a bell-shaped curve characterized by two parameters: μ and σ. Fig. 5 shows typical Gaussian density curves (Gdc) with different mean μ and standard deviation σ values obtained for different sample spaces, $\Omega_{1,2} = \{x_1, x_2, \dots, x_n\}$. As represented in Fig. 4, the curve is symmetric around μ which determines the distribution's position, and σ is a measure of dispersion around μ which characterizes the curve's spread. By means of the Gaussian distribution, the approximate probability of load variation values lying within any interval can be determined. Then, the probability of any load variation that can be satisfied by the PV source can be determined by adjusting the Δ_p value as a parameter that is used to define the interval.

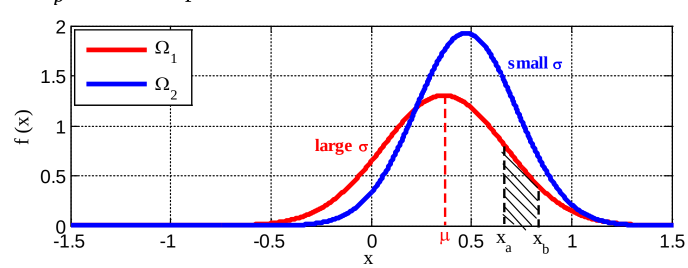

Figure 5. Gaussian density curves for different sample spaces Ω.

Table I shows two different probability levels where Δ_{p1} and Δ_{p2} values are set to μ+2σ and μ+σ, respectively. The probability levels shown in Table I are considered as reliability levels, which are named as level-1 and level-2 for different Δ_p values. The number of reliability levels can be increased by selecting different Δ_p values. In this study, two reliability levels have been analyzed.

This article has been accepted for publication in a future issue of this journal, but has not been fully edited. Content may change prior to final publication. Citation information: DOI 10.1109/TIA.2015.2499287, IEEE Transactions on Industry Applications

TABLE I. PROBABILITY TABLE FOR DIFFERENT INTERVALS

Reliability Stage	**Potential Interval**	**Probability, *P(x)***
Level-1	[-∞ , Δ_{p1}]	% 97.65
Level-2	[-∞ , Δ_{p2}]	% 87.15

Figure 6 (a) shows example load variation data in different data sets representing different load intervals. As stated earlier, the load variations in each data set have been modeled as random variables and have been used to observe the Gaussian probability distribution of the load variations at different load intervals. Finally, optimal Δ_p values for different intervals have been determined based on the user-defined reliability levels.

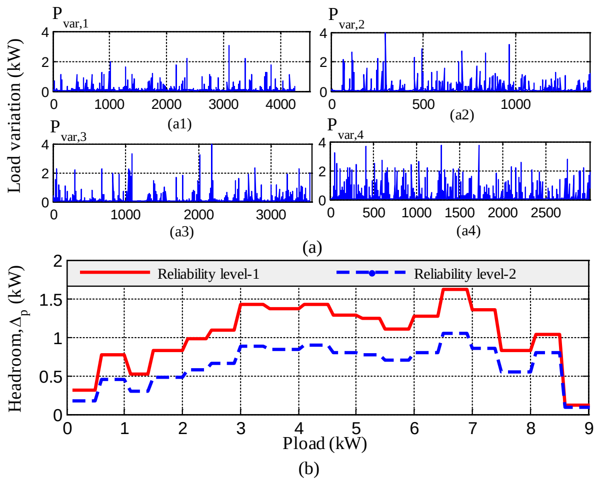

Figure 6. (a) Load variations for different load intervals (a1) [0-0.5kW], (a2) [0.5-1kW], (a3) [1-1.5kW], (a4) [1.5-2kW] and (b) the headroom value versus load demand curves for different reliability levels.

Figure 6(b) presents the optimal Δ_p values at all loading conditions determined for different reliability levels. As seen in Fig. 6(b), Δ_p values are required to be high to achieve more reliable operation of the PV sources that can cover any sudden possible load variation at any loading condition. To observe the relation between reliability and energy cost, the effect of Δ_p on the operating cost of the PV-FC system needs to be analyzed. This task is performed in the following subsection.

C. Economics of PV and FC

The cost of the energy generated by a system is determined by considering three elements: capital cost (C_{cap}), operation and maintenance cost ($C_{O\&M}$), and fuel cost (C_{fuel}). The cost ($/kWh) for renewable (non-fuel burning) energy systems is simply obtained by dividing the annual cost of the system ($C_{x,ann}$) by its annual energy output ($W_{x,ann}$) [31-33]. For dispatchable sources, there is an additional running cost ($C_{x,run}$) that corresponds to C_{fuel}. Therefore, the total electricity cost of the configured system can be determined as,

$$C_{pv-fc} = \frac{C_{pv,ann}}{W_{pv,ann}} + \frac{C_{fc,ann}}{W_{fc,ann}} + C_{fc,run} \qquad (2)$$

where C_{pv-fc} is the cost of the PV-FC microgrid system. The annual cost for both sources can be calculated as

$$C_{x,ann} = C_{cap}\left[C_{O\&M} + \frac{r_{int}}{1-(1+r_{int})^{-N}}\right] \qquad (3)$$

where r_{int} is the real interest rate and N is the estimated system lifetime. The O&M cost is usually given as a percentage of the capital cost, which is assumed to be 2% in this paper. The annual energy is calculated based on the type of energy source. Since power production of a PV is highly dependent on solar radiation (λ), the annual energy generation of a PV system is expressed as,

$$W_{pv,ann} = \sum_{n=1}^{365}\sum_{nx=1}^{24} P_{mpp,\lambda_{nx}} \qquad (4)$$

where n and nx represent the day and the hour, respectively. The daily energy calculation has been made based on the assumption that the PV is always tracking the MPP at any insulation level. Therefore, $P_{mpp,\lambda_{nx}}$ is the maximum power output at a certain insulation level. The hourly average insulation data over one year can be obtained for the PV deployment location. The annual energy of the FC system ($W_{fc,ann}$) is determined by the relation:

$$W_{fc,ann} = P_{fc}\ 8760\ cf \qquad (5)$$

where P_{fc} is the FC rated power and cf is the capacity factor that is defined as the ratio between the actual generated energy and the maximum energy produced at full rated power operation. The capacity factor is suggested to be selected between 0.15 and 0.5 for changeable load profiles [33]. Apart from the fixed electricity cost calculated by dividing the annual cost by the annual energy, the running cost is taken into account for fuel burning energy systems. The running cost of an FC system is formulated as,

$$C_{fc,run} = (C_{fuel} h_{2cons} \eta_{fc,rated})/(P_{fc,rated}\eta_{fc}) \qquad (6)$$

where C_{fuel} is the hydrogen cost (in *$/m³*) and η_{fc} represents system efficiency of the FC, which is a function of the FC operating power as shown in Fig. 7. h_{2cons} is the amount of hydrogen consumption in m^3 per hour at rated power $P_{fc,rated}$, and the corresponding system efficiency is represented by $\eta_{fc,rated}$.

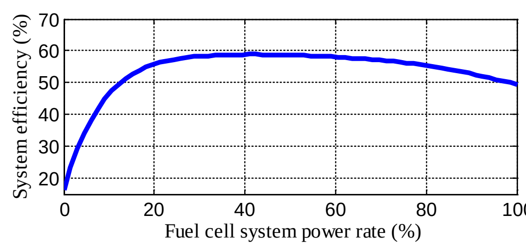

Figure. 7 Fuel cell system power versus efficiency [34].

This article has been accepted for publication in a future issue of this journal, but has not been fully edited. Content may change prior to final publication. Citation information: DOI 10.1109/TIA.2015.2499287, IEEE Transactions on Industry Applications

As stated earlier, the PV sources have zero running cost and any deviation of the PV output power from the MPP will yield a decrease in the productivity of the PV source. Hence, the energy cost of a PV system can be expressed as a function of Δ_p as below

$$C_{pv,\Delta_p} = \left(\frac{C_{pv,ann}}{W_{pv,ann}}\right)\frac{P_{mpp,\lambda_{nx}}}{P_{mpp,\lambda_{nx}} - \Delta_p} \tag{7}$$

To investigate the effect of Δ_p on the energy cost in a microgrid system, Eqn. 2 is rearranged as following;

$$C_{pv-fc} = \left(\frac{C_{pv,ann}}{W_{pv,ann}}\right)\frac{P_{mpp,\lambda_{nx}}}{P_{mpp,\lambda_{nx}} - \Delta_p} + \frac{C_{fc,ann}}{W_{fc,ann}} + C_{fc,run} \tag{8}$$

The variation of total energy cost can be observed by changing Δ_p, which will affect the power sharing between the sources at certain load demands as shown in the following equations.

$$P_{pv} = P_{mpp,\lambda_{nx}} - \Delta_p \tag{9}$$

$$P_{fc} = P_{load} - P_{mpp,\lambda_{nx}} + \Delta_p \tag{10}$$

where P_{load} and λ_{nx} is kept constant as Δ_p is changed in a certain range. Based on the determined Δ_p variation range, Δ_p versus electricity cost curves are achieved at different power demands as shown in Fig. 8(a).

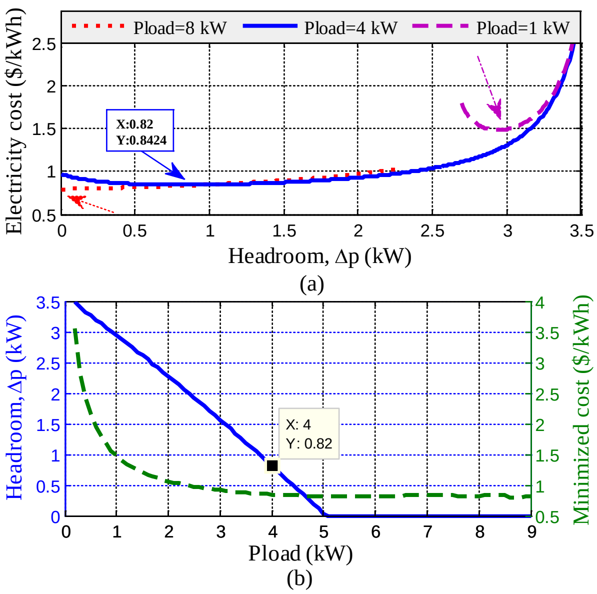

Figure 8. (a) Electricity cost versus headroom for load demands 1kW, 4kW and 8kW and (b) the headroom power and minimized electricity cost values versus load demand at $\lambda = 1\text{kW/m}^2$.

This procedure should be repeated for all possible loading conditions at different insulation levels to record all Δ_p values corresponding to the minimum cost values. The arrows in Fig. 8(a) points to the different minimum cost values for different load demands at an insulation level of $1\ kW/m^2$. Although the PV system does not require fuel, a Δ_p is required at a certain P_{load} to minimize the total operating cost as illustrated by the solid curve in Fig. 8(a). This is because the FC system efficiency rapidly increases when the FC output power is varied in the range of [0, 20% power rate] as shown in Fig. 7. If the FC output power varies in that particular range of power rate, the decrease rate in the FC energy cost becomes faster than the increase rate in the PV energy cost. The Δ_p values corresponding to minimum energy cost value have been saved for all possible loading conditions while keeping the constraint functions in consideration to achieve the solid curve shown in Fig. 8(b). The dashed curve shows the minimized cost for different loading conditions. Table II shows the cost parameters of the PV and FC technologies.

TABLE II. COST PARAMETERS OF PV AND FC SOURCES

Technology	Capital Cost [$]	O&M Cost [$]	Life Time [yrs]	Fuel Cost [$/m³]	Interest rate
Photovoltaic	16800	2%	20	N/A	5%
Fuel Cells	30000	2%	5	0.455	5%

Δ_p versus P_{load} curves obtained from reliability and total energy cost evaluation are shown in Fig. 9. At low P_{load} values, Δ_p must follow the cost curve to satisfy the constraint functions. Although Δ_p values on the reliability level-1 curve also satisfy the constraint functions after P_{load} values of 2.6 kW, the optimal Δ_p values are desired to follow the Δ_p values on the cost curve until the crossing point because they introduce higher Δ_p values corresponding to the minimum cost at the same P_{load}. After the crossing point the optimal Δ_p values must follow reliability curves to meet the user-defined reliability level.

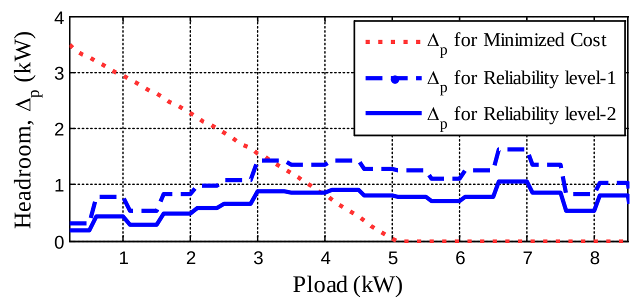

Figure 9. Headroom values versus load demand curves obtained from reliability and cost analysis.

To keep the desired optimal Δ_p value at any loading condition, PV and FC sources must follow the power-deployment lines. One way to achieve that is through central management units that observe the load and send signals to the PV and FC sources to adjust their produced power. However, since the considered system could be operated in an islanded mode, a frequency droop controller can be used to operate the microgrid system at a desired reliability level and to stabilize the system frequency.

D. Economic Analysis of ESSs

In renewable sources based microgrids, any excessive power is usually stored in ESSs. The overall system efficiency is intended to be improved with the usage of ESSs; however, the high capital cost of ESSs could be an impeding factor which may

This article has been accepted for publication in a future issue of this journal, but has not been fully edited. Content may change prior to final publication. Citation information: DOI 10.1109/TIA.2015.2499287, IEEE Transactions on Industry Applications

increase the total energy cost of the system. Accordingly, the economical impact of an ESS is investigated for the microgrid considered in this subsection. To investigate the cost impact of ESSs on the total energy cost, the battery is taken as an example of an ESS since it is a widely used storage device in the PV-FC based microgrid systems [5], [11]-[14]. Among different battery types, the most widely used one, lead-acid batteries, will be evaluated in this paper. Some characteristics of lead-acid batteries are listed in Table III. Other types of batteries could be considered as well, and the cost evaluation concept remains the same.

TABLE III. CHARACTERISTICS OF LEAD-ACID BATTERIES [35]-[38]

Characteristics	Lead-acid Battery
Efficiency	70–84%
Cycle Life [(a)]	700 @ 80% DoD - 1500 @ 33% DoD
Life time [(b)] [yrs]	2 - 4
O&M Cost [(c)] [$]	2% , 10%
Interest rate	2% - 7 %
Initial Cost [(d)] [$/kWh]	120

(a) The range of cycle life mainly depends on the type of the lead-acid battery and depth of discharge (DoD) [35], [37].

(b) Replacement timeframe is estimated assuming one cycle per day.

(c) Maintenance cost is given only for two types of lead-acid batteries: Sealed (2%) and Valve-regulated (10%) [38].

(d) Since the initial cost changes according to the cycle life, here initial cost value is given for a specific cycle life as 1000 @ 50% DoD [36], [38].

Based on the insolation levels and the characteristics of a selected PV technology, the PV power profiles at MPP operation is calculated for each day as demonstrated in Fig. 10. Figure 11 shows the comparison between a typical load and PV power profiles for a specific day in summer season. The shaded area in Fig. 11 shows daily excess energy, W_e, generated by the PV source during daytime, which can be stored in a battery and then used when there is a demand.

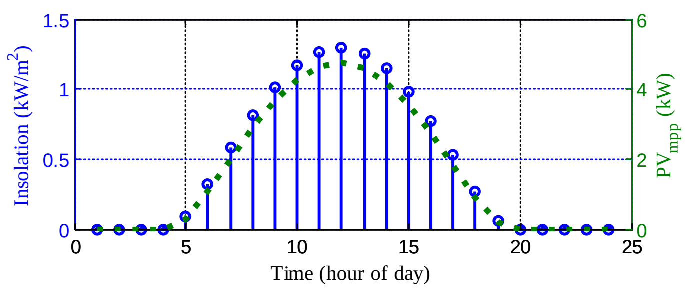

Figure 10. Daily average insolation and corresponding power generation from selected PV at MPP operation.

In the case of integrating a battery into the considered microgrid, there will be an additional annual cost $C_{b,ann}$ for the battery, which can be calculated using Eqn. 3. Since the capital cost of the battery depends on its energy capacity, required capacity needs to first be determined considering the load and PV power profiles in the considered microgrid. Here, battery capacity is chosen in such a way that the battery should be capable of storing all excess energy produced by the PV source every day to avoid wasting energy. The maximum excess energy, $max\,\{W_{e,n}\}|_{n=1,2,\ldots,365}$, in the studied case has been found to be 36.2 kWh for a day in the summer season. After taking the healthy state of charge range (typically, 10% - 90%) into account, the required capacity of the battery system has been found to be 45.25 kWh.

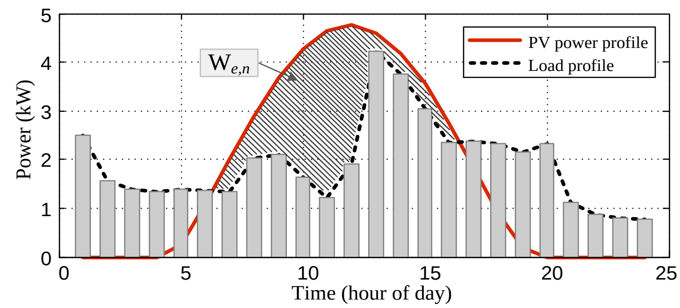

Figure 11. Typical hourly average load profile and PV power profile for a selected day in summer season.

A battery system has been chosen for the microgrid based on calculated energy capacity and chosen lead-acid battery type. The specifications of the considered battery system are listed in Table IV, from which $C_{b,ann}$ value has been found to be $2730. The energy cost of the battery system can be determined by,

$$C_{bat} = \frac{C_{b,ann}}{W_{e,ann}\eta_{bat}} \tag{11}$$

where η_{bat} is the battery efficiency, $W_{e,ann}$ is the annual excess energy produced by the PV source which can be simply calculated as,

$$W_{e,ann} = \sum_{n=1}^{365} W_{e,n} \tag{12}$$

where $W_{e,n}$ is the excess energy produced by the PV source on the n-th day of the year.

TABLE IV. PARAMETERS OF SELECTED BATTERY SYSTEM [35]-[38]

Battery type	Pack Capacity [kWh]	Amount	Capital Cost [$]	O&M Cost [$]	Life Time [yrs]	Interest rate	Efficiency
VRLA[(a)]	2.4 (200V,12Ah)	19	5470 [(b)]	10%	2.74 [(b)]	5%	75%

(a) VRLA: Valve-regulated lead-acid battery

(b) These values are given considering 1000 cycle life at 50% DoD.

The lack of a battery will cause an additional energy cost because of the wasted excess PV energy. When this excess energy is not utilized when needed, it will be compensated by the FC. Therefore, the cost of the wasted excess energy can be directly related to the running cost of the FC defined in Eqn. 6. As concluded from the results shown in Fig. 8, the FC is dictated to operate at more than 10% of its rated power to increase its efficiency (see Fig. 7), and consequently, minimize the overall cost. Therefore, the FC efficiency parameter, η_{fc} in Eqn. 6 can be set to an average constant value of around 0.55 to determine the FC running cost. Moreover, the cost of the PV source operated at MPP is calculated as $C_{pv,mpp} = C_{pv,ann}/W_{pv,ann}^{mpp}$ where $W_{pv,ann}^{mpp}$ is the annual energy produced by the PV source operating at MPP, in order to investigate whether PV installation is more cost effective than installing a battery storage system.

TABLE V. ENERGY COSTS OF PV, FC, AND BATTERY SYSTEM IN THE CONSIDERED MICROGRID

Source / storage type	**PV** (3.6 kW @ 1 kW/m^2)	**FC** (6 kW)	**Battery** (45.6 kWh)
Energy Cost ($/kWh)	0.1527 [(a)]	0.296 [(b)]	0.5625

[(a)] The energy cost given here is for PV source operated at MPP, $C_{pv,mpp}$.

[(b)] The energy cost given here is FC running cost, $C_{fc,run}$.

As seen from the results listed in Table V, calculated energy cost of the considered battery system is higher than the FC running cost (or wasted excess energy cost) and the energy cost of the PV source. Thus, the PV-FC system combined with a battery system introduces higher energy cost than the PV-FC system for the studied case in this paper. It can be concluded that installation of a battery system could be more costly under certain scenarios, as it is investigated for the considered case in this paper. The economic analysis of a PV-FC system with/without battery has been covered in this subsection under the assumption that the selected PV source performs at MPP operation. In the following subsection, the cost effect of the non-MPP operation will be investigated in detail and compared with the battery's annual cost.

E. Economic Analysis of the PV source at non-MPP Operation

In this subsection, the cost effect of moving the PV operation from the MPP is studied in detail to find out the cost effective region of a PV source operating at non-MPP with a headroom power. Figure 12 represents PV power productions in a day at different modes of operations. The dashed red line represents the power profile of a PV source operated away from the MPP by a headroom power Δ_p, which is selected as a certain percentage of $P_{mpp,\lambda_{nx}}$. From Fig. 12, the difference between the two curves is the amount of PV power available to be utilized to support variations in load and PV power production whenever needed. As the amount of the selected headroom power is increased, the PV source can satisfy more drastic variations; however, in turn, the operation cost of the PV source may increase considerably. Therefore, the cost effect of the non-MPP operation needs to be investigated in detail.

As seen in Fig.12, the PV source operating at non-MPP sacrifices an energy amount of W_{Δ_p} every day. In addition to W_{Δ_p} , the excess energy of the PV source operating at non-MPP $W_e^{non-mpp}$ is wasted due to the absence of the storage device. Considering the PV sources operating together with a storage device, the energy equivalent to the summation of W_{Δ_p} and $W_e^{non-mpp}$ can be stored for later use. Therefore, the cost of this wasted energy needs to be taken into account while formulating the cost increase caused by the non-MPP operation under the absence of the storage device. As discussed in the previous subsection, the cost of wasted energy has a direct relation with the running cost of the FC, $C_{fc,run}$. Accordingly, the cost increase from the non-MPP operation $C_{non-MPP}$ ($) can be expressed as following,

$$C_{non-MPP} = C_{fc,run}\left(W_{\Delta_p,ann} + W_{e,ann}^{non-mpp}\right) \tag{13}$$

where $W_{\Delta_p,ann}$ is the annual energy difference between the PV source operated at MPP and at non-MPP operations. The value of $W_{\Delta_p,ann}$ is calculated as the summation of $W_{\Delta_p,n}$ for $n = 1,2,\dots,365$. The other energy term $W_{e,ann}^{non-mpp}$ is the annual excess PV energy at non-MPP operation, which is calculated similar to $W_{\Delta_p,ann}$ as the summation of $W_{e,n}^{non-mpp}$ values for $n = 1,2,\dots,365$. To determine the cost effective region of the PV source operating at non-MPP, $C_{non-MPP}$ is calculated for different headroom values and compared with the annual cost of a battery whose lifetime has been assumed as 4 years. As seen in Fig. 13, the PV source operating at non-MPP is cost effective as long as the selected headroom power is less than 34.6% of maximum available PV power. Using the same approach, the cost effective area can be determined for different type of batteries performing under different operating conditions.

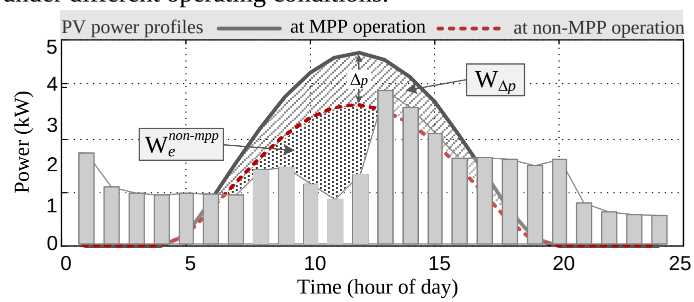

Figure 12. Daily PV source power production at the modes of MPP and non-MPP operations.

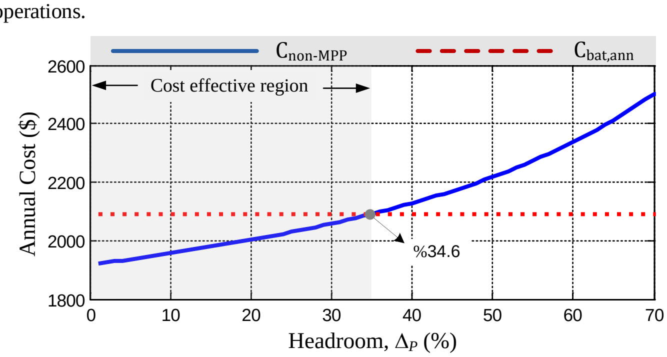

Figure 13. The behavior of $C_{non-MPP}$ corresponding to the headroom power variation.

III. FREQUENCY DROOP CONTROL

The frequency droop controller is utilized in islanded microgrids to achieve desired load sharing among the

This article has been accepted for publication in a future issue of this journal, but has not been fully edited. Content may change prior to final publication. Citation information: DOI 10.1109/TIA.2015.2499287, IEEE Transactions on Industry Applications

participating sources by regulating the frequency of the sources based on the active power [39]. If the PV and FC sources are considered, the frequency droop relations for both sources can be expressed by the following equations:

$$f_x = f_{pv} = f_{ref} - k_{pv}P_{pv} \tag{14}$$

$$f_x = f_{fc} = f_{ref} - k_{fc}P_{fc} \tag{15}$$

where the f_{ref} and f_x represent the reference and real values of the system frequency, respectively, while k_{pv} and k_{fc} values are, respectively, the droop control coefficients for the PV and FC systems. In frequency droop control, the frequencies are regulated lower as the power demand increases. The decrease in the phase of the sources results in a decrease in real output power, which introduces a negative real power feedback in the control loop. The frequency droop control scheme is constrained by the rated power of the sources since the sources operating at their rated power should not exceed the minimum acceptable frequency (f_{min}) [23]. Figure 14 demonstrates the frequency droop where the droop control coefficients are chosen as constant parameters to achieve a linear power sharing. In linear frequency droop, the power sharing ratio of the sources stays constant for all loading conditions. However, the required output power of PV and FC sources may nonlinearly change as the load demand changes. As a result, the power sharing ratio ($m(P_{load})$) between PV and FC sources could be nonlinear and expressed by arranging Eqns. 14 and 15 as,

$$m(P_{load}) = P_{fc}/P_{pv} \tag{16}$$

Based on the obtained power-deployment lines, the power sharing ratio can be determined for all possible loading conditions. It will be shown in the following section that the power sharing ratio can be effectively used to achieve the desired power sharing among the sources.

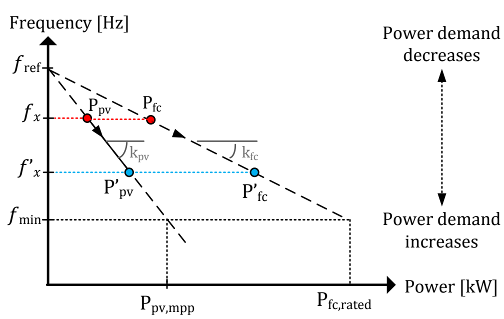

Figure 14. Frequency variations of the sources corresponding to the power demand in a linear droop control mechanism.

IV. Simulation and Experimental Results

In this section, the PV-FC based microgrid depicted in Fig. 3 is studied to verify the effectiveness of the proposed method. Based on the parameters given in Table I, the optimal Δ_p values for reliability level-1 have been obtained as shown in Fig. 15.

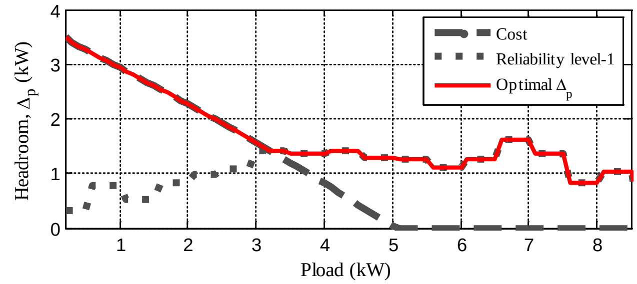

Figure 15. Optimal headroom at different load demands for reliability level-1.

To maintain the desired Δ_p value at any loading condition, the PV and FC sources must follow the power-deployment lines shown in Fig. 16(a). To establish such nonlinear power sharing, the droop control coefficients are defined as $k_{fc} = c$ and $k_{pv} = m(P_{load})c$, where c is a constant droop coefficient that is defined based on the minimum acceptable frequency. Figure 16(b) shows the power sharing ratio curve, which has been obtained based on the determined power-deployment lines. Here, $m(P_{load})$ is used as a dynamic parameter to adjust the k_{pv} according to the load demand change, so that the PV and FC sources are ensured to follow their power-deployment lines shown in Fig. 16(a).

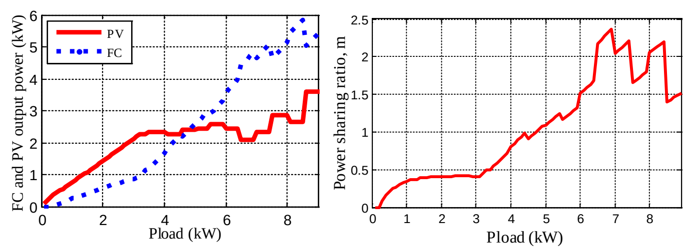

(a) (b)

Figure 16. (a) Power-deployment lines for PV and FC sources and (b) power sharing ratio curve.

A simulation study has been conducted here to verify the effectiveness of the presented droop scheme in maintaining the optimal Δ_p value at any loading condition. To illustrate the advantage of the presented droop scheme, linear (conventional) droop scheme has also been simulated. In the linear droop control case, the power sharing ratio m has been set to 1.0. The models of PV and FC modules proposed in [5] and [25] have been used in simulations to analyze the performance of the proposed droop scheme under the dynamic effects of the PV and FC sources. The simulation was made for a PV-FC based microgrid system that feeds a common resistive load. The load profile has been changed as shown in Fig. 17 to observe the Δ_p value at different power sharing levels. The variation of PV-FC output power and Δ_p are presented in Figs. 18 and 19, respectively.

This article has been accepted for publication in a future issue of this journal, but has not been fully edited. Content may change prior to final publication. Citation information: DOI 10.1109/TIA.2015.2499287, IEEE Transactions on Industry Applications

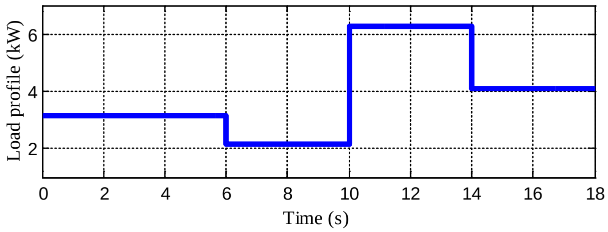

Figure 17. Simulated load profile.

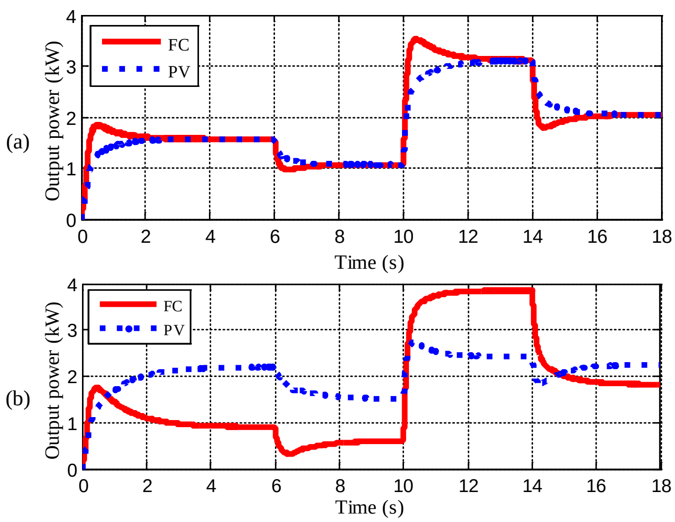

Figure 18. Output power behavior of FC and PV sources under (a) linear and (b) nonlinear droop control.

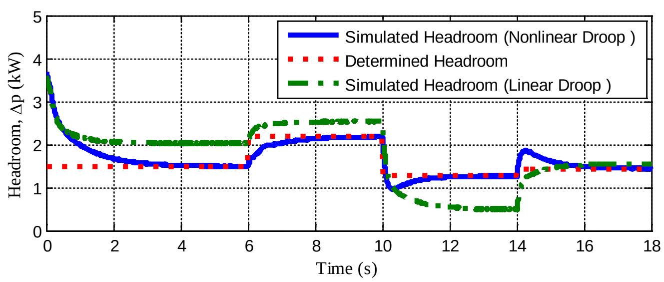

Figure 19. PV headroom power variation under linear and nonlinear droop control.

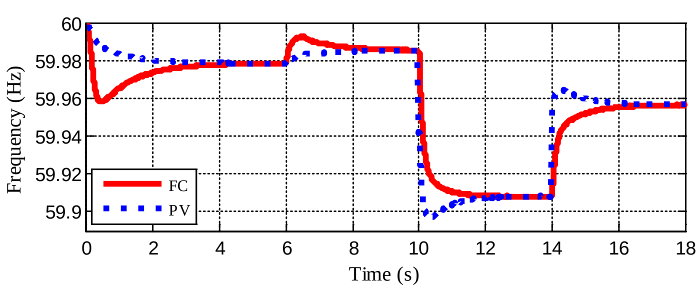

Figure 20. Frequency variation of PV and FC sources.

Here, the constant droop coefficient is set to 0.00015 and the insulation level is considered to be $1\ kW/m^2$. Figure 18(a) shows power sharing among the PV and FC sources. As expected, an equal sharing has been realized since the value of m was set to 1.0 to investigate the performance of linear droop control. Although linear droop control provides stable power management among the participating sources, it does not satisfy the determined headroom power as shown in Fig. 19. On the other hand, the power sharing ratio between the sources changes nonlinearly corresponding to P_{load} variations when the nonlinear droop scheme is performed as seen in Fig. 18 (b). Thus, Δ_p exactly tracks the headroom values determined for reliability level-1 as shown in Fig 19. At any P_{load} variation, source frequencies are first disturbed to different values and then smoothly converge to the same value at steady state as shown in Fig. 20.

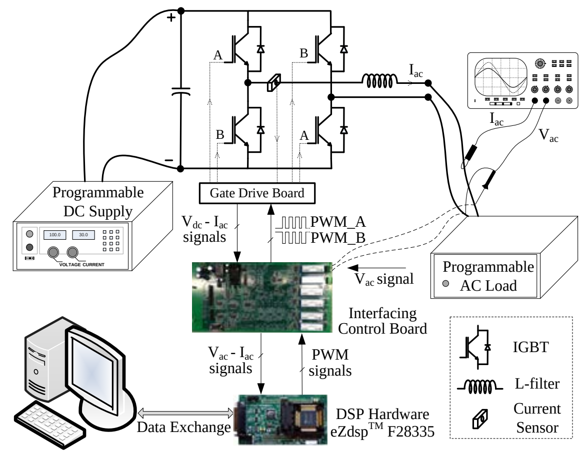

Figure 21. Schematic of a single phase source in the experimental bench.

In this paper, an experimental study has also been conducted on the University of Akron microgrid test bed (UA-MGTB) to verify the feasibility of nonlinear power sharing using the proposed droop scheme. As shown in simulation results, the dynamics of the PV and FC sources do not affect the performance of the proposed droop scheme. Therefore, the DC bus of the PV and FC sources have been simply imitated using programmable DC sources (PDCS). A simple setup is considered in this study to provide verification for the concept. However, the setup complexity does not affect the method validity. The method depends on frequency droop, which is a universal signal and depends on the power dynamics which are much slower than the current dynamics in power system lines. Thus, the structure of the experimental setup should not have an impact on the reached conclusions.

Figure 21 shows the schematic of a single phase source in the MGTB. Each PDCS in the MGTB is connected to a single phase inverter. The inverter output is connected to a Programmable AC load (PACL) through an L-filter to reduce the harmonics on the

This article has been accepted for publication in a future issue of this journal, but has not been fully edited. Content may change prior to final publication. Citation information: DOI 10.1109/TIA.2015.2499287, IEEE Transactions on Industry Applications

AC bus voltage. In this study, an L filter has been chosen since it is the simplest filter in terms of its design. To be able to obtain a sufficient harmonic attenuation, L-filters have been made with high inductance. Accordingly, experimental tests in this study have been limited to low power levels with the purpose of limiting the voltage drop effect of the large inductance. However, improved filters such as LC or LCL filters are highly recommended to be used in similar topologies in order to achieve better performance from the experiments which need to be run at high power levels. Excitation signals for the inverter is provided from a Texas Instruments DSP through an interfacing control board. A communication link between a host computer and the target DSP board is established by a JTAG Emulator and parallel port cable to load the control routine on the DSP and swap data throughout the experiment. Figure 22 shows the experimental setup of one of the inverter units in the MGTB.

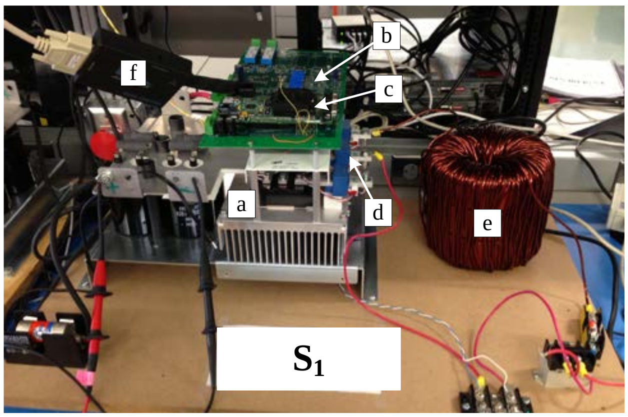

Figure 22. Experimental setup : (a) Inverter unit, (b) Interfacing control board, (c) DSP board, (d) Current sensor, (e) L-filter, and (f) JTAG Emulator.

Here, two PDCSs are utilized to imitate the DC bus voltage of PV and FC sources. The inverter units are connected to the PACL at the point of common coupling (PCC) through the low pass filters as shown in Fig. 23. For the purpose of providing voltage quality related functions such as voltage regulation and harmonic compensation, the filter topology shown in Fig. 23 can be used. However, the experimental test in this study was limited to power sharing analysis for which the L-filter is prone to be sufficient. To observe the nonlinear power sharing between the sources, the power demand of the microgrid system is changed by controlling the PACL through the host computer.

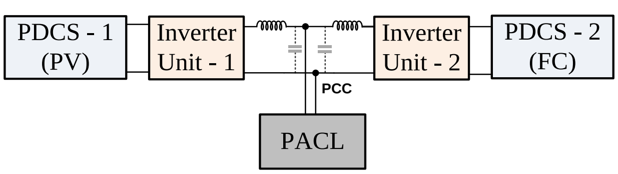

Figure 23. Configuration of the experimental setup.

A wide range of loads have been applied to the system in order to test the performance of the proposed droop scheme. The current waveforms of the PV and FC sources as well as the load current are shown in Fig. 24. Figure 25 shows the voltage waveform at PCC. As seen, the current and voltage waveforms are proper and the PCC voltage is well-regulated. The operating frequency is smoothly stabilized after each load variation. The power sharing among the sources is shown in Fig. 26. Clearly, a nonlinear power sharing is realized when the proposed droop scheme is implemented. As opposed to the linear droop case, the power sharing ratio *m* varies subsequent to the load variation based on the power sharing ratio curve shown in Fig. 16 (b). It must be noted that the load power range in the power sharing ratio curve in Fig. 16(b) goes up to a maximum of 9 kW; however, the experimental test setup is limited to 4 kW. Therefore, the power sharing ratio cannot be directly used in the experiment. Because of that, the load data in the power sharing ratio was first scaled down by a factor of two and then used in the experimental tests.

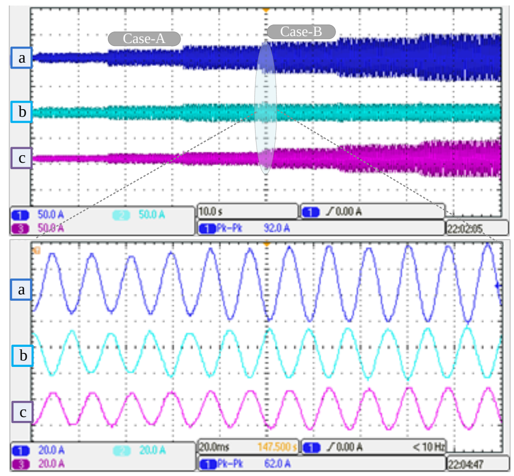

Figure 24. Experimental measurements: (a) Load current, (b) PV current, and (c) FC current.

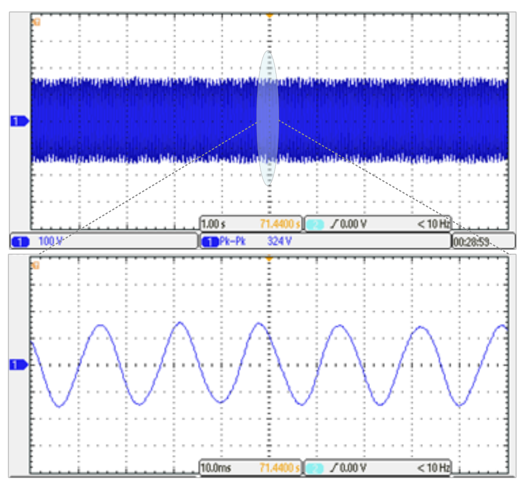

Figure 25. Voltage waveform at PCC.

To have a clear comparison with the results in Fig. 16, the obtained experimental results shown in Fig. 26 have been scaled

This article has been accepted for publication in a future issue of this journal, but has not been fully edited. Content may change prior to final publication. Citation information: DOI 10.1109/TIA.2015.2499287, IEEE Transactions on Industry Applications

up by a factor of two. As seen in Fig. 26, the PV source is providing more power than the FC at low loadings, as desired (see Fig. 16(a)). On the other hand, the FC starts delivering more power at high loadings (> 4.8 kW). Most significantly, the optimal power sharing ratio (see Fig. 16(b)) at each loading is achieved with a slight discrepancy as shown in Fig. 27. The detailed experimental measurements are listed in Table VI for two of the different loading conditions. As expected from Fig. 16(b), the power sharing ratio is expected to be almost 0.54 and 1.28 at 3.5 kW and 5.8 kW power demands, respectively. The power sharing ratio calculated from the experimental results almost satisfy the desired power sharing ratio at tested loadings. Accordingly, the optimal power sharing curve obtained through the proposed optimization procedure can be effectively used in the proposed droop scheme to allocate the desired PV headroom irrespective of load variations. From the simulation and experimental results it can be concluded that the proposed droop scheme can be used to achieve desired reliability and cost effectiveness for the PV-FC based microgrid system operation.

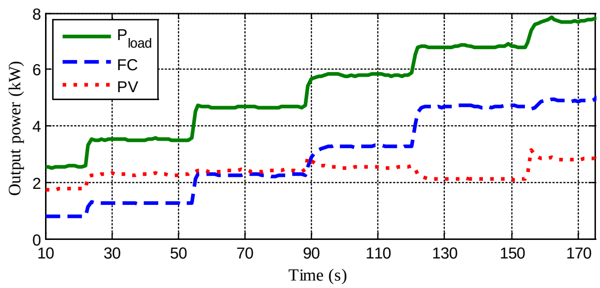

Figure 26. Output power variations of the PV and FC sources corresponding to the loading steps.

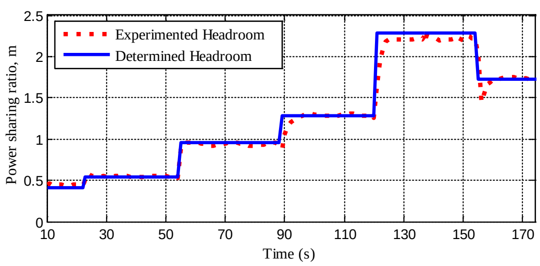

Figure 27. Power sharing ratio variation corresponding to the load change.

TABLE VI. EXPERIMENTAL RESULTS

Power Demand	Source Type	Source Current [A rms]	AC Bus Voltage [V rms]	Supplied Power [kW]	System Frequency [Hz]	Power sharing ratio, *m*
Case A	PV	≈ 9.83	≈ 116	≈ 1.14	59.95	0.544
	FC	≈ 5.35		≈ 0.62		
Case B	PV	≈ 11.34	≈ 112	≈ 1.27	59.91	1.283
	FC	≈ 14.6		≈ 1.63		

V. CONCLUSION

The reliability and cost aspects of the PV-FC based microgrid system have been investigated under the limitations of the system's operation to perform optimal reserve assessment. The PV energy production is allowed to deviate from MPP such that it can have energy reserve to support sudden load variation. The PV source has been operated with a headroom power to increase the reliability of the microgrid system. Since the headroom power impacts the system cost, it has been optimized to achieve a desired reliability level while minimizing the running cost of the microgrid system. Moreover, having a headroom in the PV energy production could reduce the cost as it allows the FC to operate at points with higher efficiencies. Based on the optimized headroom power, power sharing between the PV and FC sources has been explored. For every loading condition, there will be two headroom values, one which minimizes the cost and the other which satisfies the required level of reliability. The proposed method selects the optimal headroom between these two determined values. Then, a nonlinear frequency droop scheme has been established and applied to the system to achieve the desired power sharing at any loading conditions without a need for a communication system. Simulation results have shown that the proposed method is effective in maintaining the optimal headroom value for minimum cost without violating the required reliability conditions.

REFERENCES

[1] International Energy Outlook 2013 Energy Information Administration, the U.S. Department of Energy Report #:DOE/EIA-0484, July 2013

[2] A. M. Omer, "Energy, environment and sustainable development," *Renew. Sustain. Energy Rev.*, vol. 12, pp. 2265-2300, 2008.

[3] P. Thounthong, V. Chunkag, P. Sethakul, S. Sikkabut, S. Pierfederici, and B. Davat, "Energy management of fuel cell/solar cell/supercapacitor hybrid power source," *J.Power Sources*, vol. 196, pp. 313-324,2011.

[4] C. S. Wang and M. H. Nehrir, "Power management of a stand-alone wind/photovoltaic/fuel cell energy system," *IEEE Trans. Energy Convers.*, vol. 23, no.3, pp. 957-967, 2008.

[5] M. Uzunoglu, O. C. Onar, and M. S. Alam, "Modeling, control and simulation of a PV/FC/UC based hybrid power generation systemfor stand-alone applications," *Renewable Energy*, vol. 34, no.3, pp. 509-520, 2009.

[6] M.O. Badawy, and Y. Sozer "Power Flow Management of a Grid Tied PV-Battery Powered Fast Electric Vehicle Charging Station," in *proc. IEEE Energy Convers. Congr. Expo. (ECCE)*, pp. 4959-4966, 20-24 Sept. 2015.

[7] M.O. Badawy, A.S. Yilmaz, Y. Sozer, and I. Husain, "Parallel Power Processing Topology for Solar PV Applications", *IEEE Trans. on Ind. Appl.*, vol. 50, no. 2, pp. 1245-1255, 2014.

[8] M.O. Badawy, A. Elrayyah, F. Cingoz, and Y. Sozer, "Non-isolated individual MPP trackers for series PV strings through partial current processing technique," in *Proc. IEEE Appl. Power Electron. Conf.*, pp.3034-3041, 2014.

[9] R.Contino, F. Iannone, S. Leva, D. Zaninelli, "Hybrid photovoltaic-fuel cell system controller sizing and dynamic performance evaluation," 2006 IEEE Power Engineering Society General Meeting, 2006.

[10] F. Ongaro, S. Saggini, and P. Mattavelli, "Li-Ion Battery-Supercapacitor Hybrid Storage System for a Long Lifetime, Photovoltaic-Based Wireless Sensor Network," *IEEE Trans. PowerElectron.*, vol. 27, no.9, pp. 3944-3952, 2012.

[11] H. H. Zhou, T. Bhattacharya, D. Tran, T. S. T. Siew, and A. M. Khambadkone, "Composite Energy Storage System Involving Battery and Ultracapacitor With Dynamic Energy Management in Microgrid

Applications," *EEE Trans. Power Electron.*, vol. 26, no.3, pp. 923-930, 2011.

[12] H. Kanchev, D. Lu, F. Colas, V. Lazarov, and B. Francois, "Energy Management and Operational Planning of a Microgrid With a PV-Based Active Generator for Smart Grid Applications," *IEEE Trans. Ind. Electron.*, vol. 58, no.10, pp. 4583-4592, 2011.

[13] D. B. Nelson, M. H. Nehrir, and C. Wang, "Unit sizing and cost analysis of stand-alone hybrid wind/PV/fuel cell power generation systems," *Renewable Energy,* vol. 31, no.10, pp. 1641-1656, 2006.

[14] Z. H. Jiang, "Power management of hybrid photovoltaic fuel cell power systems," *IEEE Power Eng. Soc. Gen. Meet.*, pp. 1-6, 2006.

[15] P. A. Lehman, C. E. Chamberlin, J. I. Zoellick, and R. A. Engel, "A photovoltaic/fuel cell power system for a remoteelecommunications station," *Conf. Rec. of the 28th IEEE Photovoltaic Specialists Conf.*, pp. 1552-1555, 2000.

[16] Y. Hidaka and K. Kawahara, "Modelling of a hybrid system of photovoltaic and fuel cell for operational strategy in residential use", Universities Power Engineering Conference (UPEC), pp. 1-6, 2012.

[17] Y. Ru, J. Kleissl and S. Martinez "Storage size determination for grid-connected photovoltaic systems", 2011.

[18] C. Codemo, T. Erseghe and A. Zanella "Energy storage optimization strategies for smart grids", *Proc. 2013 IEEE Int. Conf. Communications (ICC)*, pp.4089 -4093

[19] Moazeni, S.; Powell, W.B.; Hajimiragha, A.H. "Mean-Conditional Value-at-Risk Optimal Energy Storage Operation in the Presence of Transaction Costs", *Power Systems, IEEE Transactions on,* On page(s): 1222 - 1232 Volume: 30, Issue: 3, May 2015

[20] P. Harsha and M. Dahleh "Optimal management and sizing of energy storage under dynamic pricing for the efficient integration of renewable energy", *IEEE Trans. Power Syst.*,

[21] M. Castaneda, A. Cano, F. Jurado, H. Sanchez and L. M. Fernandez, "Sizing optimization, dynamic modeling and energy management strategies of a stand-alone PV/hydrogen/battery-based hybrid system," International Journal of Hydrogen Energy, vol. 38, no10, pp. 3830-3845, April 2013.

[22] M. S. ElNozahy and M. M. A. Salama, "Technical impacts of grid-connected photovoltaic systems on electrical networks-A review," *J. Renewable and Sustainable Energy,* vol. 5, 2013.

[23] R. H. Lasseter, "MicroGrids," *Proc. IEEE Power Eng. Soc. Winter Meet.*,pp.305-308,2002.

[24] W. D. Kellogg, M. H. Nehrir, G. Venkataramanan, and V. Gerez, "Generation unit sizing and cost analysis for stand-alone wind, photovoltaic, and hybrid wind/PV systems," *IIEEE Trans. Energy Convers.*, vol. 13, no.1, pp. 70-75, 1998.

[25] H. L. Tsai, C. S. Tu, and Y. J. Su, "Development of Generalized Photovoltaic Model Using MATLAB/SIMULINK," *World Congr. on Eng. and Comput. Sci.*, pp. 846-851, 2008.

[26] A. Elrayyah, Y. Sozer, and M. Elbuluk, "Control of Microgrid-Connected Pv-Sources," *IEEE Ind. Appl. Soc. Annu. Meet. (IAS)*, 2012.

[27] M. G. Villalva, J. R. Gazoli, and E. Ruppert, "Comprehensive Approach to Modeling and Simulation of Photovoltaic Arrays," *IEEE Trans. Power Electron.*, vol. 24, no.5, pp. 1198-1208, 2009.

[28] C. S. Wang, M. H. Nehrir, and S. R. Shaw, "Dynamic models and model validation for PEM fuel cells using electrical circuits," *IEEE Trans. Energy Convers.*, vol. 20, no.2, pp. 442-451, 2005

[29] M. Tanrioven and M. S. Alam, "Reliability modeling and analysis of stand-alone PEM fuel cell power plants," *Renewable Energy*, vol. 31, pp. 915-933, 2006.

[30] M. Uzunoglu and M. S. Alam, "Dynamic modeling, design, and simulation of a combined PEM fuel cell and ultracapacitor system for stand-alone residential applications," *IEEE Trans. Energy Convers.*, vol. 21, no.3, pp. 767-775, 2006.

[31] B. van der Zwaan and A. Rabl, "Prospects for PV: a learning curve analysis," *Solar Energy*, vol. 74, no.1, pp. 19-31, 2003.

[32] R. Ramakumar, N. G. Butler, A. P. Rodriguez, and S. S. Venkata, "Economic-Aspects of Advanced Energy Technologies," *Proc. IEEE*,vol. 81, no.1, pp. 318-332, 1993.

[33] F. Barbir and T. Gomez, "Efficiency and economics of proton exchange membrane (PEM) fuel cells," *Int. J. Hydrogen Energy*, vol. 21, no.10, pp. 891-901, 1996.

[34] K. S. Jeong and B. S. Oh, "Fuel economy and life-cycle cost analysis of a fuel cell hybrid vehicle," *J.Power Sources*, vol. 105, no.1, pp. 58-65, 2002

[35] J.L. Sullivan and L. Gaines, "Status of life cycle inventories for batteries,". *Energy Convers. Manage*., vol. 58,pp. 134-148, 2012.

[36] G. Albright, J. Edie, and S. Al-Hallaj, "A Comparison of Lead Acid to Lithium-ion in Stationary Storage Applications", *AllCell Techn. LLC*, 2012.

[37] C. J. Rydh and B. A. Sanden "Energy analysis of batteries in photovoltaic systems. Part I: Performance and energy requirements", *Energ. Convers. Manage.*, vol. 46, no. 11/12, pp.1957 -1979, 2005

[38] S. Anuphappharadorn, S. Sukchai, C. Sirisamphanwong, and N. Ketjoy, "Comparison the economic analysis of the battery between lithium-ion and lead-acid in PV stand-alone application," *Energy Procedia 11th Eco-Energy and Materials Sci. and Eng. (11th EMSES)*, vol. 56, pp.352-358, 2014.

[39] B. B. K. D. Brabandere, J. V. Keybus, A. Woyte, J. Driesen, R. Belmans, "A voltage and fequency droop control method for parallel inverters," *IEEE Trans. Power Electron.*, vol. 22, no.4, pp. 1107-1115, 2008.